Nucleation theory applied to polymer crystals with curved edges*

Robert L. Miller and John D. Hoffman†
Michigan Molecular Institute, 1910 W. St. Andrews Road, Midland, MI 48640, USA
(Received 23 February 1990; revised 5 April 1990; accepted 19 April 1990)

The nucleation-based theory of polymer crystal growth has been extended to apply to the growth rate and morphology of polyethylene (PE) single crystals with curved edges. The treatment is employed to analyse in detail the data of Organ and Keller on PE crystals formed from n-hexadecane and n-tetradecanol, which possess both {1 1 0} and {2 0 0} sectors; the subordinate {2 0 0} sectors exhibit the curved edge. The theory (1) introduces the concept of lattice strain in the {2 0 0} sectors through a parameter σ_s (which has an independent justification), (2) takes a {2 0 0} growth front to have the energetics associated with its being 'serrated' on a molecular level in addition to being strained, and (3) treats the dominant {1 1 0} growth front in terms of the energetics of the customary Lauritzen–Hoffman 'flat-surface' nucleation model. For the correct σ_s, the theory accurately predicts the aspect ratio and curvature as a function of crystallization temperature for each solvent. The treatment provides insights relating to (1) the different melting points, fold surface energies, angles of tilt and fold surface regularities of the {1 1 0} and {2 0 0} sectors, (2) the prediction of an upper limit T_{max} above which such crystals will not form, (3) the occurrence of a regime I → II transition on the {1 1 0} growth front and its absence on the {2 0 0} front, and (4) the reason that both melt- and solution-crystallized PE exhibit a preference for ***b*** axis growth. The proposed treatment removes an objection to nucleation theory and, with appropriate modifications, is potentially useful in treating morphological problems in other systems.

(Keywords: polymer crystallization; nucleation theory; polyethylene; single crystal; dilute solution; curved edge; lattice strain; chain folding; serrated growth front; regime transition)

INTRODUCTION

Approximately 30 years ago, Lauritzen and Hoffman (LH) proposed a nucleation-based theory to account for the rate of growth of lamellar polymer crystals and for the variation in thickness of such crystals with undercooling for both melts and solutions[1]. Subsequent modifications and improvements to this general type of theory have been made, including the effect of fluctuations of the fold period[2,3], the effect of reptation on the growth rate[4,5], the melting behaviour[6], a preliminary approach to dealing with the 'quantized' fold periods exhibited by low-molecular-weight fractions[7] and the consideration[8–11] of different 'regimes' of crystallization. The LH approach, as extended and improved by its originators as well as others, has permitted one to understand and to interpret a variety of measurements related to isothermal crystallization in a broad range of polymers (see, for example, refs. 12 and 13 and the references cited above). To date, it would appear that no alternative approach has been proposed that has been able to deal with as many different aspects of the polymer crystallization problem.

The original LH theory was developed solely for relatively high-molecular-weight polymers *and* for the fastest growing crystal front (the dominant growth face), which was assumed to be flat in the macroscopic sense, though some local roughness (on a molecular level) resulting from random nucleation events was postulated. Occasionally, these limitations have been ignored and the basic LH theory applied to cases for which it was patently unsuited. As a consequence, the inconsistent and/or misleading results obtained were sometimes considered to arise from an invalidity of the nucleation approach to polymer crystal growth with chain folding. One such example—the existence of polyethylene (PE) single-crystal lamellae with curved edges—is the subject of this work. Our overall objective is to demonstrate how nucleation theory may be modified and extended to apply also to this particular behaviour.

It has long been recognized that crystallization of PE from dilute xylene solution may give rise to 'truncated' single-crystal lamellae exhibiting both {1 1 0} and {2 0 0} faces (and sectors), each sector exhibiting an essentially straight edge for aspect ratios less than about 2. The classical LH theory[12] considers that a face, once nucleated, should fill out rapidly and completely. Hence, the LH treatment leads to the macroscopically straight edges commonly seen in such crystals. Aspect ratios of truncated lamellae were determined as a function of concentration and of crystallization temperature by Valenti and Pedemonte[14], and were analysed in terms of LH nucleation theory in the 'straight-edge' region by Passaglia and Khoury[15] and by Passaglia and DiMarzio[16].

In addition, lamellae with decidedly curved edges were observed in dilute-solution-grown PE single crystals by Keith[17] and subsequently many others (see e.g. ref. 15 for an extensive bibliography). Curved edges were also

* MMI contribution number 366
† Present address: Department of Materials Science and Engineering, The Johns Hopkins Univesity, Baltimore, MD 21218, USA

0032-3861/91/060963-16

observed in melt-crystallized PE preparations by LaBaig, Keith *et al.* and Bassett *et al.*[17]. Toda[18,19] suggested that the solvent acting as an impurity interrupts substrate completion and causes the curvature effect, whereas Sadler[20] proposed a 'roughening' mechanism. In any case, we shall shortly describe a nucleation-based treatment that is designed to be applicable to chain-folded PE crystals formed in both the melt and dilute solution and which (when tested for the case of solution-grown crystals of PE) leads to a quantitative understanding of the curvature effect and to insights into a number of related phenomena as well.

It had been suggested that the existence of lamellar crystals with curved edges indicated a fundamental flaw in nucleation theory, including specifically the LH treatment (Sadler[20] and references cited therein). Sadler clearly posed a valid question when he cited the apparent incompatibility of a curved-edge crystal and the original LH nucleation theory, which features a macroscopically flat surface. Note that the faces in PE single-crystal lamellae exhibiting curvature are the slower growing subordinate {2 0 0}, and not the faster growing dominant {1 1 0}, types. Application of the 'classical' LH theory to a macroscopically curved facet, as well as any conclusions drawn therefrom, is clearly invalid. Since nucleation theory leads to satisfactory results when applied to the dominant 'straight-edged' growth faces, we deemed it likely that a variant of this type of theory, which took account of the different characteristics of the subordinate growth faces, would provide the most acceptable solution to the puzzle. One must expect major differences in the surface energetics of the two types of growth front. We shall represent subordinate {2 0 0} growth faces in PE crystals as 'serrated' on a molecular level to bring out the feature that little or no lateral surface free energy σ is involved in the work required to add a 'first' stem to such a face. At the same time we retain the conventional 'flat-surface' model as a description of the dominant {1 1 0} growth front to highlight the concept that a relatively large 'σ' term is then involved in putting down a 'first' stem. The occurrence of polymer crystals with curved edges is not restricted to PE. There are a number of polymers whose lamellar crystals apparently exhibit such curvature: for example, polyacrylonitrile[21], *trans*-1,4-polyisoprene[22] and (possibly) extended-chain crystallization of poly(ethylene oxide) fractions[23].

Only recently have data adequate for an understanding of the curved-edge behaviour become available. Organ and Keller[24,25], from a comprehensive study of the growth of PE single-crystal lamellae from dilute solution in n-hexadecane and n-tetradecanol, have provided the basis on which to test a model to explain this phenomenon, which is discussed below. Their study, at fixed concentration, is thus far unique in that a regime I → II transition[8–10,12,26] was detected in the growth kinetics of the dominant {1 1 0} faces for crystals grown from a solvent.

Additional input to the formulation of the model came from the crystallography of PE preparations. Bassett[27] determined for an isolated lamella that the diagonals of the PE unit cell were unequal ($d_{110} \neq d_{1\bar{1}0}$) and that the asymmetry alternated from one sector to another. Davis *et al.*[28] established that the PE unit-cell dimensions were a function of the lamellar thickness. Such observations clearly indicated the presence of strain within the crystals, quite probably resulting from the repulsion of chain folds. We shall account for the presence of strain in the crystal proper by introduction of a quantity denoted σ_s. Marand[29] has summarized arguments indicating that the lattice expansion occurs mainly between {2 0 0} planes, which are nominally parallel to the growth face in those sectors which exhibit the curved edges. He also determined on the basis of molecular energy calculations that σ_s was of the order of 1 erg cm^{-2} (1 mJ m^{-2}). In view of the above, we deemed it appropriate to modify nucleation theory to include lattice strain as a part of the explanation of the curved-edge phenomenon. Thus, in treating the subordinate {2 0 0} sector with its curved edge, we shall take into account the presence of lattice strain as well as the fact that the growing edge may be represented in energetic terms as 'serrated' on a molecular level. It will emerge that a determination of the behaviour of the substrate completion rate for a {2 0 0} sector, g_{200}, is critical to an understanding of the phenomenon of lamellae with curved edges. Another point is the suggestion on the basis of the 'decoration' technique that the 'fold' surfaces of the {2 0 0} sectors are more disordered than those of the {1 1 0} sectors[30].

Our understanding of the existence of lamellae with curved edges within the confines of nucleation theory benefited from the cooperative efforts of others. Mansfield[31,32] provided a set of phenomenological relations connecting the geometry of a curved-edge PE crystal and the various growth and substrate completion rates critical to its formation, and, as noted earlier, Marand established the approximate magnitude of the lattice strain parameter σ_s. We earlier[33] developed a model based on nucleation theory for a serrated growth face where the underlying crystal (represented for simplicity as having a square lattice) possessed lattice strain, and we presented preliminary results for PE crystallized from n-hexadecane. Here, we describe in detail the application of the model to the results of Organ and Keller for crystallization of PE from both n-hexadecane and n-tetradecanol. It will emerge that the value of σ_s derived from the curvature data is quite similar to that predicted on the basis of molecular energy calculations.

The treatment extends beyond that of simply fitting the curvature data. It yields supportable values of the lattice strain energy and of the fold surface free energy in the sectors with curved edges, and accurately reproduces shapes and axial ratios of the crystals as a function of crystallization temperature. It predicts, and preliminary evidence supports, the existence of an upper temperature limit above which crystals of the type considered here cannot form. The theory indicates that, partly or largely because of the lattice strain, the {2 0 0} sectors may melt at a measurably lower temperature than will the {1 1 0} sectors. The treatment is also consistent with the angle of tilt of the chains being larger in the body of the {2 0 0} sectors than in the {1 1 0} and with the 'fold' surface regularity being better in the {1 1 0} sectors than the {2 0 0}. Finally, we note for these curved-edge crystals that a regime I → II transition appears on a {1 1 0} face whereas application of the Lauritzen 'Z_L' test[9] to growth on the corresponding curved {2 0 0} face reveals it to be consistent with regime II behaviour in the entire range of measurement. Thus, we suggest that a crystal of this type can exhibit different regime behaviour on crystallographically dissimilar faces at the same growth temperature.

ANALYSIS OF LAMELLAR SHAPES: GROWTH AND SUBSTRATE COMPLETION RATES

We indicate here the method of analysis employed to extract the substrate completion rate for the {2 0 0} sectors, g_{200}, from observed growth rate and shape data of PE single crystals as a function of growth temperature. The behaviour of g_{200} relative to the rate of advance of a {2 0 0} face, G_{200}, is key to the selection of the relevant nucleation model, which is described in the next section.

We begin with an analysis of shape data based upon the somewhat idealized PE single-crystal lamella shown in *Figure 1*. Such a crystal contains six sectors—four {1 1 0} and two {2 0 0}—and its shape may be defined in terms of its aspect ratio (A_r) and the curvature (C) of the edges of the {2 0 0} sectors. The aspect ratio is defined as the ratio of the length and the width or as the ratio of the growth rate at the tip and the growth rate of the curved face[15,16]. That is:

$$A_r \equiv G_{110(tip)}/G_{200} = G_{110}/(G_{200} \cos \Lambda) \quad (1)$$

where Λ is the angle between the normal to a {1 1 0} growth plane and the horizontal direction and is fixed by the crystallography of the unit cell ($\Lambda = \tan^{-1}(|\boldsymbol{b}|/|\boldsymbol{a}|)$, where $\boldsymbol{a}$ and $\boldsymbol{b}$ are the unit-cell vectors). (Previously[15], this angle was denoted by the symbol θ.) Note that $A_{r(min)} = |\boldsymbol{b}|/|\boldsymbol{a}|$ describes the conventional diamond-shaped lozenge as commonly obtained from crystallization of PE from a dilute xylene solution. The curvature may be defined as the ratio of the 'bulge' of a {2 0 0} face and the length of the base of that face. In terms of *Figure 1*:

$$C \equiv K_2/2ht \quad (2)$$

where h is the rate of advance (in a horizontal direction) of the intersection between adjacent {2 0 0} and {1 1 0} faces and t is the elapsed time. In *Figure 1*, the angle θ characterizes the shape of the growing sector and is a measure of the increase in length of each (2 0 0) layer over the previous one.

In a crystal that might be represented by *Figure 1*, growth of the dominant {1 1 0} growth faces is normal, i.e. governed by the 'classical' LH flat-surface theory[12]. A subordinate 'curved' {2 0 0} growth face has edgewise advance rate h, forward advance rate G_{200}, and substrate completion rate g_{200}. Growth of each {2 0 0} sector, therefore, occurs under conditions wherein its boundaries are moving. From classical (flat-surface) nucleation theory[12], one expects the condition $g_{200} \gg h$ to hold, which would lead to a flat growth profile.

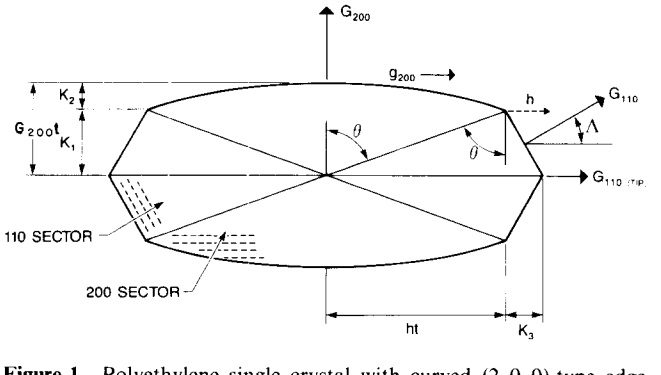

Figure 1 Polyethylene single crystal with curved (2 0 0)-type edge (schematic). Broken lines symbolize fold planes. (From Hoffman and Miller[33] after Mansfield[31].) See text for detailed description

To understand the situation depicted in *Figure 1* in terms of nucleation theory, one must be able to relate the geometry (shape) observed to the pertinent growth rates. Mansfield[31] obtained phenomenological equations for this problem by solving the differential equations for nucleation and growth given by Frank[10] for the case with moving boundaries. For purposes here, his results are summarized briefly. First, Mansfield defined a dummy variable ϕ by:

$$\cos \phi \equiv h/g_{200} \quad (3)$$

which is valid for $h \leqslant g_{200}$. Then he obtained as steady-state solutions[31,32] the following relations between parameters characteristic of the ideal crystal illustrated in *Figure 1* and the relevant rates of growth:

$$\tan \theta = h/(G_{200} \sin \phi) \quad (4)$$

$$h = G_{110}/\cos \Lambda - G_{200} \tan \Lambda \sin \phi \quad (5)$$

$$C = (G_{200}/2h)(1 - \sin \phi) \quad (6)$$

and

$$A_r = (h/G_{200})(1 + \tan \Lambda/\tan \theta) \quad (7)$$

Combination and rearrangement of the above yields:

$$\tan \theta = (\tan \Lambda - A_r)/(2CA_r - 1) \quad (8)$$

and

$$C \tan \theta = (1 - \sin \phi)/(2 \sin \phi) \quad (9)$$

Equations (3)–(9) were derived on the basis that multiple nucleation occurred on the curved {2 0 0} edge so that growth conformed to regime II, the actual substrate length L being $2ht$. No restrictions forbidding a regime I → II transition on the {1 1 0} front were introduced.

From known Λ and measurements of A_r, C and $G_{110(tip)}$ as a function of temperature, one may determine the behaviour of G_{110}, G_{200}, g_{200}, h and θ for the system being studied. Clearly, when $g_{200} \gg h$ in the above, $\sin \phi \to 1$ and $C \to 0$, which is the expectation of classical LH theory[12] for a flat growth profile. On the other hand, given Λ, G_{100}, G_{200} and g_{200} for a lamellar crystal exhibiting curvature, one must solve a parametric expression (such as equation (5)) for h, since ϕ depends on h, following which the geometrical parameters pertinent to *Figure 1* may be calculated.

Organ and Keller[25] studied the growth (at various isothermal temperatures) of single-crystal lamellae from dilute (0.05% weight/volume) solutions of PE in n-hexadecane and in n-tetradecanol. Their results are reproduced in *Figures 2* (growth rates) and *3* (C and A_r). *Figure 2* also includes earlier work on the growth of single crystals from xylene. In these figures, T_x and ΔT_x are, respectively, the isothermal crystallization temperature and the corresponding degree of undercooling ($\Delta T_x = T_d - T_x$, where T_d is the dissolution temperature of PE in the particular solvent). Below we shall show that the analysis of these data in terms of our model with the serrated edge and lattice strain quantitatively reproduces their experiments and allows predictions in agreement with other observations.

In *Figure 2* it can be seen that the {1 1 0} faces exhibit a regime I → II transition in two of the solvent systems. (The regime I → II transition relates only to these faces—see later.) The solvent commonly used to study the growth of PE single crystals—xylene—does *not* display a regime transition in the temperature range investigated

to date, nor do the crystals exhibit curved edges in the temperature range depicted in *Figure 2*. Because of the latter, the data for this solvent cannot be analysed to obtain $g_{200}(T)$.

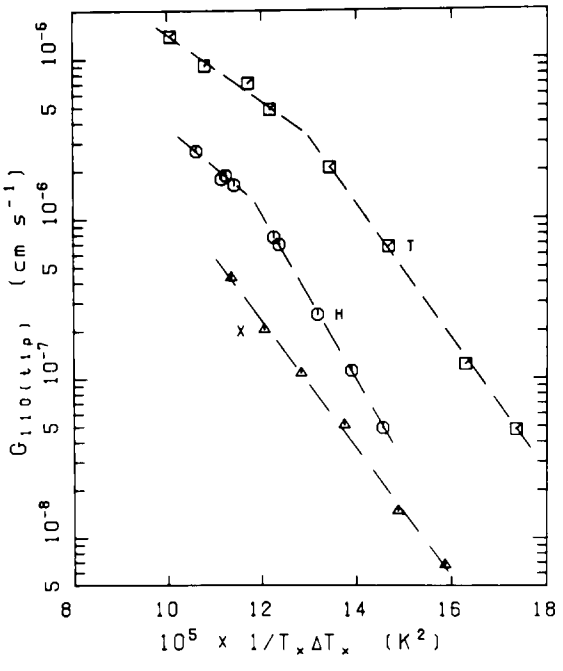

Figure 2 Growth rate $G_{110(tip)}$ of polyethylene single-crystal lamellae as a function of $1/T_x\Delta T_x$ (after Organ and Keller[25]): (Δ) 0.1% in xylene; (○) 0.05% in *n*-hexadecane; (□) 0.05% in *n*-tetradecanol

The analysis proceeded in the following manner. The growth rate of the dominant {1 1 0} sectors was obtained from the data in *Figure 2* and from $G_{110} = G_{110(tip)} \cos \Lambda$, where $\Lambda = 32.9°$ based upon the unit-cell dimensions listed in *Table 1*. The growth rate G_{200} of the subordinate {2 0 0} sectors was obtained from G_{110} and A_r by means of equation (1). The Organ and Keller data of *Figure 3* could then be analysed readily by means of the Mansfield relations. Equation (8) gave values of tan θ which, with equation (9), yielded values of ϕ (hence, h/g_{200}), leading to values of h/G_{200} (hence, h) by way of equation (4). Finally, equation (3) was used to obtain g_{200}. Thus, the phenomenological parameters important for the formation of curved edges (h, θ and, most importantly, g_{200}) were deduced directly from the experimental observations.

The results of our analysis of the data in *Figures 2* and *3* for the two solvents are shown in *Figures 4* and *5*. The upper part of each figure displays the growth rate of the dominant {1 1 0} sectors and exhibits the regime I → II transition shown in *Figure 2*. The lower part of each figure displays the growth rate G_{200} and substrate completion rate g_{200} for the subordinate {2 0 0} sectors. No regime transition is apparent in the $G_{200}(T)$ curves or in the appropriate plots of ln G_{200} involving $1/T\Delta T_s$ to be discussed subsequently. Thus, we take it to be possible for different faces of a growing crystalline lamella to correspond to different regimes, an inference that will in due course be supported by application of the Lauritzen 'Z_L' test[9], which shows that $G_{200}(T)$ is consistent with regime II. Values of θ for each temperature and solvent obtained as part of this analysis are in

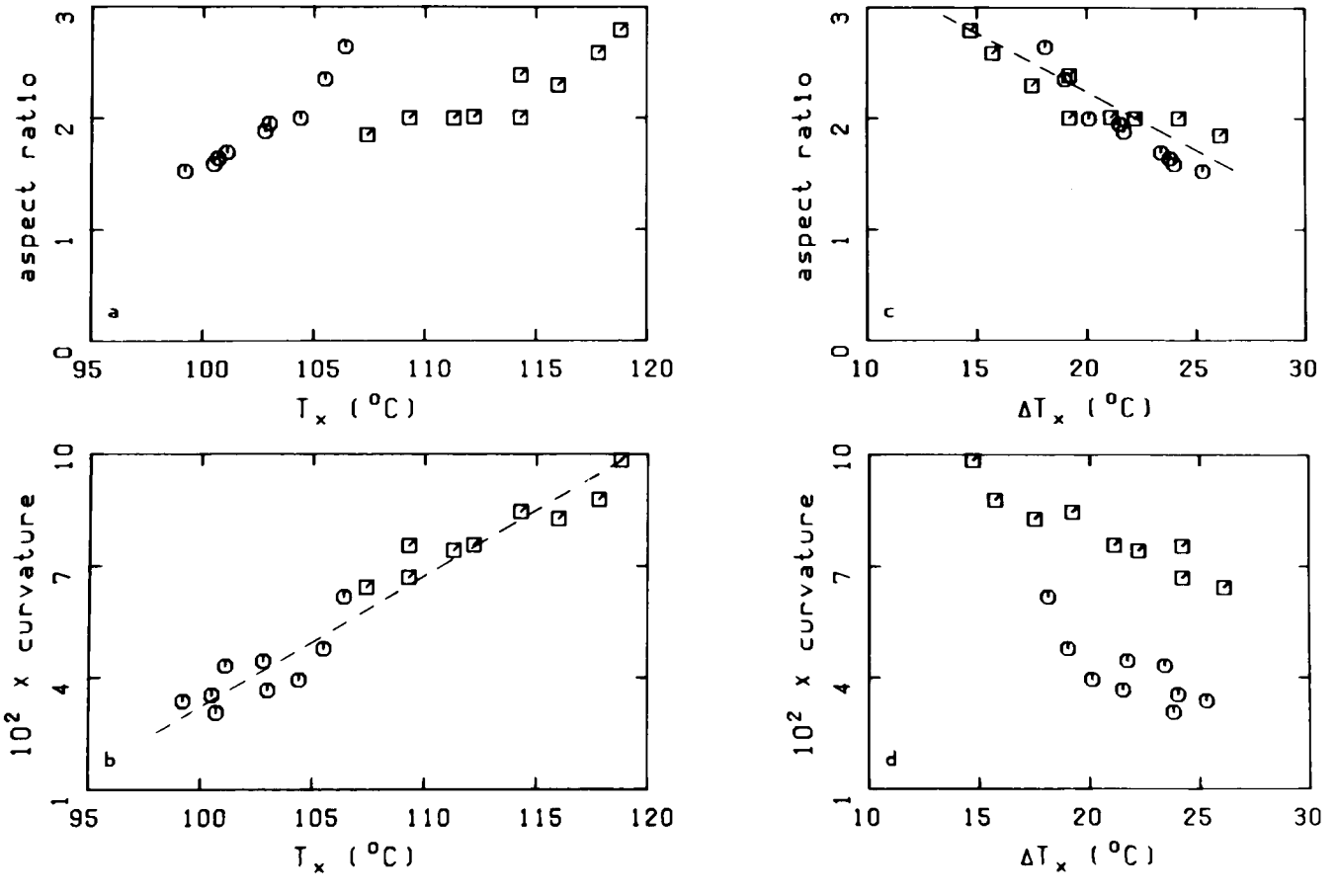

Figure 3 Aspect ratio A_r and curvature C of polyethylene lamellae as a function of crystallization temperature T_x and of undercooling ΔT_x (after Organ and Keller[25]): symbols as in *Figure 2*. (a) A_r *versus* T_x; (b) C *versus* T_x; (c) A_r *versus* ΔT_x; (d) C *versus* ΔT_x

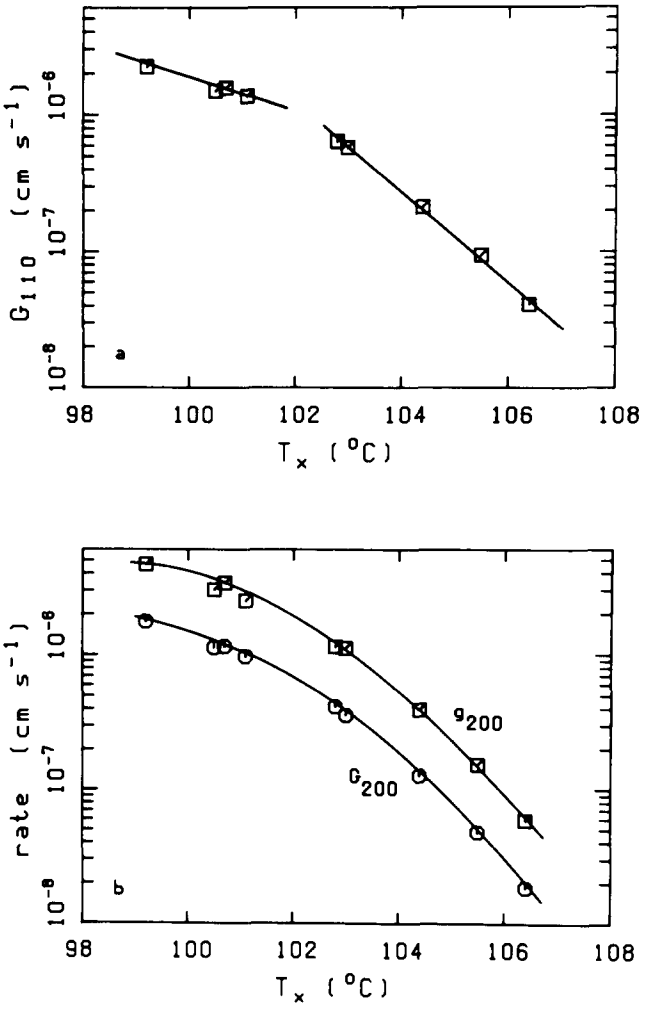

Figure 4 Growth and substrate completion rates as a function of crystallization temperature T_x for polyethylene single crystals of the type illustrated in *Figure 1* grown from a 0.05% solution in n-hexadecane. (a) Growth rate G_{110} of the dominant {1 1 0} faces. Note the regime I → II transition associated with these faces. (b) Growth rate G_{200} and substrate completion rate g_{200} of the 'curved' {2 0 0} faces

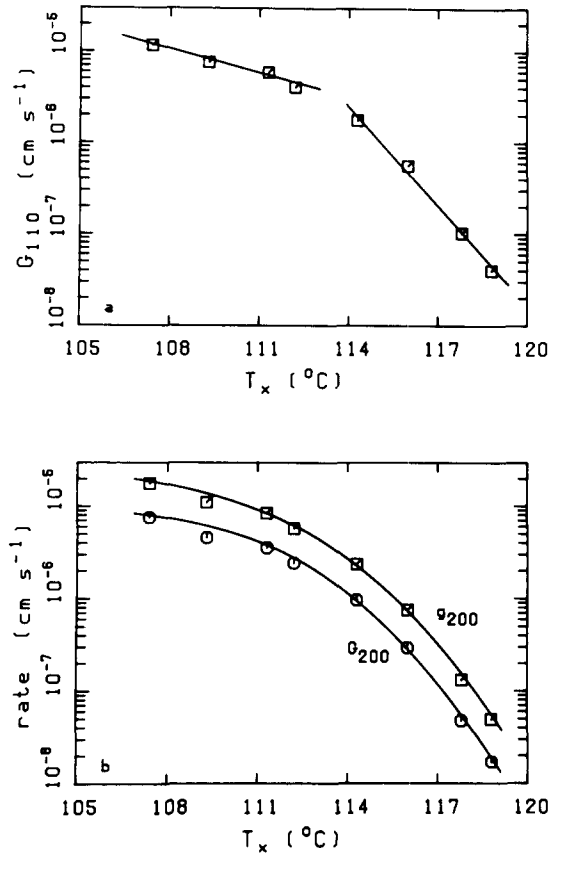

Figure 5 As in *Figure 4* but for n-tetradecanol

excellent agreement with those which can be measured from the figures presented by Organ and Keller[25].

From *Figures 4* and *5* it can be seen that the phenomenological analysis for crystals with curved edges leads to essentially parallel behaviour of G_{200} and g_{200} (even through the temperature of the regime I → II transition for the dominant face). This will prove to be decisive in the selection of the correct nucleation model for the {2 0 0} sectors.

Any model of the mechanism of growth of {2 0 0} sectors with curved edges must meet three criteria indicated by the above: (a) predict the curved edges; (b) predict the nearly parallel growth and substrate completion rates for the sectors with curved edges; and (c) correspond to regime II behaviour for growth of the {2 0 0} sectors over the experimental temperature range. The origin and consequences of these constraints are discussed briefly below.

Curvature of a growing face is described by equation (6) in which the primary variable is the quantity $(1 - \sin \phi)$. By inference, then, for the {2 0 0} faces to exhibit curvature, the substrate completion rate g_{200} must be just slightly faster than is the edge advance rate h: otherwise, $(1 - \sin \phi)$ will be small and detectable curvature will vanish. This conclusion is emphasized in *Figure 6* in which the variation of $\sin \phi$ with h/g_{200} is shown. Clearly curvature will be detectable only for a restricted range of h/g_{200}, say, $0.3 \leqslant h/g_{200} \leqslant 1.0$. Through equation (5), the main contribution to the value of h is G_{110} (which is independent of the nature of the growth process in the {2 0 0} sectors). Accordingly, if curvature is to be exhibited, we require that g_{200} be reduced markedly from what on a flat unstrained surface would be a high value. One way to accomplish this is to

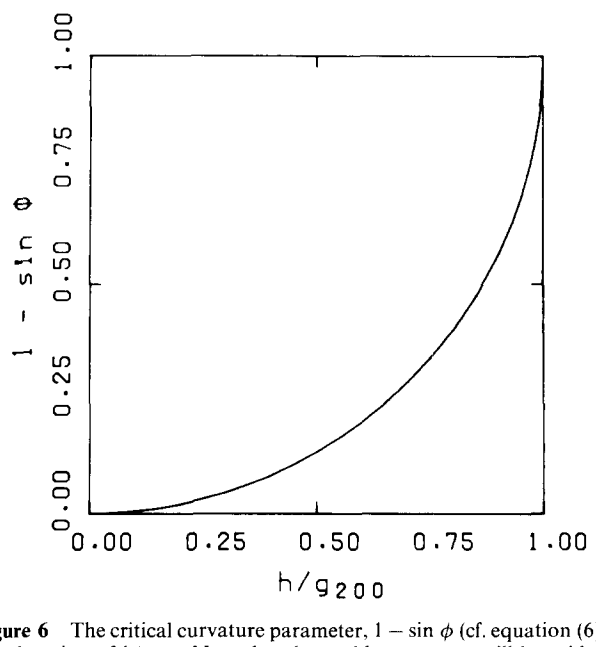

Figure 6 The critical curvature parameter, $1 - \sin \phi$ (cf. equation (6)), as a function of h/g_{200}. Note that detectable curvature will be evident only for the limited range for h/g_{200} of approximately $0.3 \leqslant h/g_{200} \leqslant 1.0$

reduce the effective melting point of the {2 0 0} sectors. Such a reduction is herein taken to be a consequence within the sectors of lattice strain whose presence was discussed above[28]. Davé and Farmer[34], from semi-empirical molecular energy calculations, concluded that {2 0 0} folds would be difficult to pack. Hence, the origin of the strain in the crystal interior may be presumed to be repulsive interaction between the {2 0 0} folds.

Parallelism of g_{200} and G_{200} for the curved edges requires complete or nearly complete elimination of the normal term involving the lateral surface free energy σ from the surface nucleation rate i, irrespective of any consideration about lattice strain. In other terms, an appropriate model must *not* permit the creation of a significant amount of exposed lateral surface in the nucleation step as is characteristic of the flat-surface model.

Criterion (c) above is imposed by the derivation of the Mansfield relations (equations (3)–(9)). Curved edges are not predicted if a substrate length L of the usual magnitude (say, $\sim 50\,\text{nm}$[26]) is introduced into the moving boundary problem. This implies that the particular type of 'defect' that might otherwise define the 'domain size' L on the {2 0 0} face is ineffective in terminating substrate completion on the {2 0 0} face, causing the operative substrate length to be $2ht$. A substrate length L of the usual magnitude is clearly operative on the {1 1 0} face causing the regime I → II transition to appear.

NUCLEATION MODEL FOR CURVED EDGES

An appropriate model involving lattice strain to suppress g and a means to eliminate the σ term is one with a serrated edge, such as is shown in *Figure 7*. (Note, in the present context, that the serration is on a *molecular level.*) This figure depicts the projection of a PE crystal onto the ***ab*** plane. The broken rectangles represent individual unit cells, the heavy full lines represent growth faces, and the lighter full lines form a grid of lozenges that represent the cross-sectional areas of previously added stems. 'Flat surfaces' corresponding to growth of the dominant {1 1 0} growth faces are shown at the right of the figure. At the top is the 'serrated surface' for a (2 0 0) face. Stems indicated by broken lozenges represent nucleation acts on each of the growth faces illustrated. Clearly, the flat-surface model includes a lateral surface energy (σ) term in the nucleation process whereas the ideal serrated surface does not. (Surfaces exposed to the surroundings, of course, are characterized by the lateral surface free energy σ. Of relevance here is that addition of a stem on the serrated face involves no net increase in σ surface whereas nucleation on the flat surface does.*)

Each stem (represented by a diamond-shaped lozenge) added to a growing surface interacts with the surface (and with adjacent stems) along a contact length s which is indicated for the (2 0 0) face by the lines of short

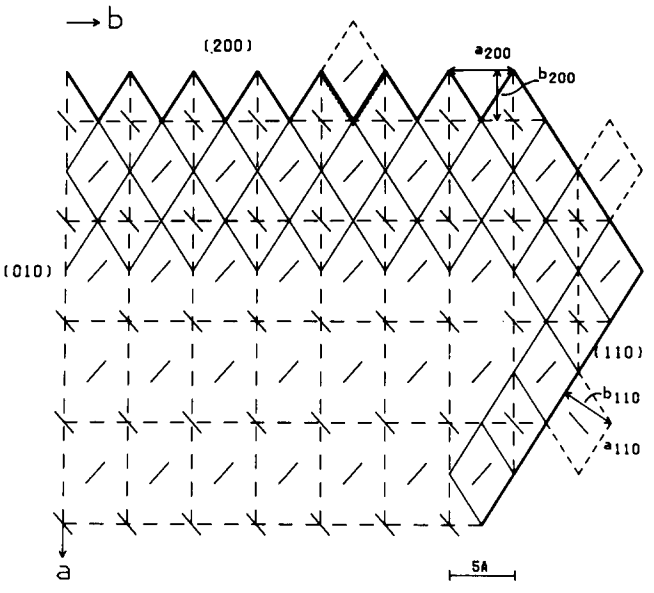

Figure 7 Lattice model (to scale) for nucleation and substrate completion in polyethylene for both the 'flat' and the 'serrated' surface cases, projected onto (0 0 1) (schematic). Note that the serration is on a molecular level. ***a***, ***b*** are unit-cell axes; a_{hk0}, b_{hk0} are stem thickness ($b_{hk0} = d_{hk0}$) and stem width (a_{hk0}) values relevant to growth on the ($hk0$) crystal plane. (\, /) traces of the planar zig-zag chain backbone; (---) unit-cell edges; (———) positions of previously added stems (the heavy lines denote the current growth surfaces); (---) surface patch denoting a nucleation act; (· · · · ·) locus of the lattice strain (characterized by surface free energy σ_s) encountered upon addition of a stem to the serrated (2 0 0) face along a total contact length (per added stem) s with contact area sl (l is the lamellar thickness). Surfaces exposed to the surroundings are characterized (as usual) by a lateral surface free energy, σ

dashes. If l is the thickness of the lamella (or, more precisely, the stem length if the chains are tilted with respect to the plane of the chain folds), the contact area between the substrate and the added stem is sl. (By adding subscripts to s to distinguish between nucleation and substrate completion processes, the model becomes quite general and one may treat both the serrated and the flat surfaces[35].) Molecular dimensions of adding stems are identified in the figure for each surface and are listed in *Table 1*. In our previous preliminary treatment[33] of the PE crystals formed in n-hexadecane, we employed a simplified 'square' lattice. The treatment to be given here is similar, but is more exact for the PE case and is general for the orthorhombic crystal system.

Interaction on the {2 0 0} faces leading to internal lattice strain is introduced by means of an interfacial surface free energy σ_s acting over the area of contact. We anticipate that $\sigma_s < \sigma$. Implicit in *Figure 7* is that growth of a flat {1 1 0} surface is treated in the conventional LH manner, i.e. without lattice strain effects.

One may treat the serrated-edge model depicted in *Figure 7* in a manner completely analogous to the standard flux equation formulation of nucleation and growth on a flat surface[33]. The free energy of adding v stems to the (2 0 0) face at the temperature $T = T_x$ may be written:

$$\Delta\phi_v = vsl\sigma_s + 2(v-1)a_0b_0\sigma_e - va_0b_0l\Delta G \qquad (10a)$$

$$= sl\sigma_s - a_0b_0l\Delta G - (v-1)a_0b_0\left(l\Delta G - 2\sigma_e - \frac{sl\sigma_s}{a_0b_0}\right) \qquad (10b)$$

* The authors naturally realize that no surface is either absolutely flat or ideally serrated. We follow here the normal convention of nucleation theory in proposing a surface geometry that pictorializes a situation consistent with the underlying crystal structure such that one can reasonably describe the corresponding surface energetics. The {2 0 0} faces may be considered to be serrated to the same approximation that one may consider the {1 1 0} faces to be flat—in the event, the major source of the important energetic differences between the two faces can thus be perceived in geometrical terms

in which a_0 (the stem width), b_0 (the stem thickness) and σ_e (the fold surface excess free energy) refer to the parameter values appropriate for the specified growing surface and ΔG is the free energy of fusion, $\Delta G = \Delta h_f \Delta T / T_m$, in the normal fashion with Δh_f the heat of fusion and T_m the strain-free thermodynamic melting point of the crystallizing system ($\Delta T = T_m - T$). As required for clarity, we shall distinguish values of the parameters for different faces.

One may construct the general rate constants for nucleation and growth that are consistent with $\Delta\phi_v$ in the standard manner[33]. For simplicity here, we choose the situation in which the backward reaction is suppressed ($\varepsilon = 0$) and set the energy apportionment factor (ψ) equal to zero. Whether the backward reaction is included or not has little effect on the resultant mathematics. The principal difference in the '$\varepsilon = 1$' (full backward reaction) and the '$\varepsilon = 0$' (suppressed backward reaction) treatments of the serrated model is in the value of δ_{200} in equation (11) below: the value of δ_{200} for the '$\varepsilon = 1$' case is twice that given in equation (11)[33]. Other differences occur in the pre-exponential factor, but these affect our analysis in only a trivial way. The meaning of ψ was discussed in our earlier paper[33], where it was noted that the mathematical approximation $\psi = 0$ led to sufficiently realistic expressions for stem lengths and the growth and substrate completion rates at low-to-moderate undercoolings. (Low values of ψ imply that the activated state in nucleation and substrate completion has a 'partial stem' character[33].) Thus, applying the flux concepts and definitions of classical LH theory[12] to the molecularly serrated model, one obtains[33] for the growing {2 0 0} sector at the crystallization temperature T, the initial lamellar thickness:

$$l_g^* = 2\sigma_{e(200)}/\Delta G_s + \delta_{200} \qquad \text{with} \quad \delta_{200} \simeq kT/s\sigma_s \tag{11}$$

the substrate completion rate:

$$g_{200} = g_{0(200)}\Delta T_s \exp(-q_{200}/kT) \times \exp(-Q_D^*/RT)\exp(-K_s/T\Delta T_s) \tag{12a}$$

the surface nucleation rate:

$$i_{200} = i_{0(200)}\Delta T_s \exp(-Q_D^*/RT)\exp(-K_s/T\Delta T_s) \tag{12b}$$

and hence the growth rate:

$$G_{200} = G_{0(200)}\Delta T_s \exp[-(q_{200}/2kT)(j-1)] \times \exp(-Q_D^*/RT)\exp(-K_s/T\Delta T_s) \tag{13}$$

where $j = 1$ for regimes I and III and $j = 2$ for regime II. (In the present case the correct choice is $j = 2$.) The nucleation constant:

$$K_s = 2s\sigma_s\sigma_{e(200)}T_m/k\Delta h_f \tag{14}$$

is the same for all three regimes. (The 'front factor' $G_{0(200)}$ is, of course, different for the different regimes.) Also, one has the usual result for the work of chain folding:

$$q_{200} = 2a_0b_0\sigma_{e(200)} \tag{15}$$

where a_0b_0 is the cross-sectional area of the chain. We define a quantity W_{200} as the *total* work of chain folding in a {2 0 0} sector. It includes q_{200} *and* the lattice strain incurred by the folding process:

$$W_{200} = q_{200} + sl_g^*\sigma_s \tag{16}$$

In the above, k is the Boltzmann constant and R the gas constant.

The presence of lattice strain lowers the melting point of a {2 0 0} sector below that resulting from lamellar thickness alone:

$$T'_{m(200)} = T_m(1 - 2\sigma_{e(200)}/\Delta h_f l_{200} - s\sigma_s/\Delta h_f a_0 b_0) \tag{17}$$

From this expression, the melting point of a large, thick crystal where $l \to \infty$ (and with strain appropriate to some finite thickness such as l_g^*) may be written as:

$$T_s = T_m(1 - s\sigma_s/\Delta h_f a_0 b_0) \tag{18}$$

and the degree of undercooling relative to the melting point of a strained sector becomes:

$$\Delta T_s = T_s - T \tag{19}$$

The free energy of fusion in the presence of strain, then, may be expressed as $\Delta G_s = \Delta h_f \Delta T_s$. Finally, for the orthorhombic lattice of PE:

$$s = 2[b_{200}^2 + (a_{200}/2)^2]^{1/2} \tag{20}$$

which, for the stem dimensions listed in *Table 1*, becomes $s = 0.91$ nm. These expressions for a {2 0 0} sector are generalizations of those presented earlier[33] for a square lattice ($a_{200} = 2b_{200}$) for which $s = 2(2)^{1/2}b_{200} = 0.87$ nm.

Note in equation (17) the term $s\sigma_s/\Delta h_f a_0 b_0$, which leads to an additional depression of the melting point caused by the presence of strain. The effect of this term is to reduce g_{200}. Of course, another factor involving σ_s that reduces g_{200} is that of K_s in equation (12a).

For future reference, analogous expressions for the strain-free {1 1 0} sectors may be written[5] according to the classical 'flat-surface' model:

$$l_{g(110)}^* = 2\sigma_{e(110)}/\Delta G + \delta_{110} \qquad \text{with} \quad \delta_{110} \simeq kT/2b_{110}\sigma \tag{21}$$

$$T'_{m(110)} = T_m(1 - 2\sigma_{e(110)}/\Delta h_f l_{110}) \tag{22}$$

$$G_{110} = C_i\Delta T \exp[-(q_{110}/2kT)(j-1)] \times \exp(-Q_D^*/RT)\exp(-K_g/T\Delta T) \tag{23}$$

in which $\Delta T = T_m - T$, $C_i \equiv C_{i(110)}$ is the 'front factor' for the ith regime, and:

$$K_{g(i)} = 4b_{110}\sigma\sigma_{e(110)}T_m/jk\Delta h_f \tag{24}$$

is the nucleation constant for the ith regime with $j = 1$ in regimes I and III and $j = 2$ in regime II as before. The substrate completion rate for the {1 1 0} sectors is:

$$g_{110} = g_{0(110)}\Delta T \exp(-q_{110}/kT)\exp(-Q_D^*/RT) \tag{25a}$$

and the corresponding surface nucleation rate is:

$$i_{110} = i_{0(110)}\Delta T \exp(-Q_D^*/RT)\exp(-K_g/T\Delta T) \tag{25b}$$

The work of chain folding, q_{110}, is given by:

$$q_{110} = 2a_0b_0\sigma_{e(110)} \tag{26}$$

As mentioned, we have used the $\varepsilon = 0$ case (suppressed backward reaction) for simplicity. The mathematical relations are little affected and expressions appropriate to the inclusion of the backward reaction may readily be obtained beginning with equation (10) and/or from the tables previously presented[33]. For crystallization from dilute solution one replaces T_m by T_d as appropriate in all of the above expressions.

Equations (12)–(19), with $j = 2$, satisfy the three requirements noted earlier. For finite σ_s, the melting point is reduced and g_{200} is slowed through the factor $\exp(-K_s/T\Delta T_s)$. From equations (12a) and (13), g_{200}

and G_{200} are seen to be essentially parallel, differing only in the minor factor $\exp(-q_{200}/2kT)$ for $j=2$. In anticipation of results to be discussed shortly, we have accepted the concept of different values of σ_e in different sectors. Alfonso *et al.*[36] suggested that fold surface free energies might be different in different fold sectors, Passaglia and Khoury[15] explicitly so stated, and Toda[37] interpreted growth rates of PE in n-octane solution in terms of the flat-surface model in which $\sigma\sigma_{e(200)} > \sigma\sigma_{e(110)}$.

For the PE lamellae with curved edges from two different solvents, one obtains the phenomenological behaviour for the {2 0 0} sectors shown in *Figures 4* and *5*, which we shall interpret with the mathematical expressions based on the strained, serrated-edge model of *Figure 7*. The corresponding data for the dominant 'flat-surface' growth {1 1 0} faces shown in the same figures are treated in the customary way with equations (23) and (24). From a visual comparison of the G_{110} and G_{200} curves in *Figures 4* and *5*, one can surmise at the outset that the effective undercooling scale for G_{200} is different from that of G_{110}, with the downturn of G_{200} being caused by a lower effective melting point. This is embodied in the theory by the use of $T_s - T$ for G_{200} and $T_d - T$ for G_{110}, this difference being justified by the strain known to be present in the {2 0 0} sectors and by the ensuing ability to predict curvature.

Definitions and acceptable values of various input parameters for PE are collected in *Table 1*. It should be noted that Organ and Keller[24] (from analyses based on equations (21) and (22)) concluded that $\sigma_{e(110)}$ should be significantly higher for n-hexadecane than for n-tetradecanol, a suggestion also indicated by the different slopes of the lines in *Figure 2*. However, Huseby and Bair's results for the solvent n-octadecane[38] and Nakajima's values for a variety of solvents including n-hexadecane[39], all obtained from T'_m *versus* $1/l$ plots, are more in agreement with the 'universal' value of 90 erg cm^{-2} that we have adopted here*. For comparison, we exhibit the behaviour with xylene as the solvent (*Figure 2*), where data are to be treated as a regime I 'flat-surface' case without significant lattice strain.

Table 1 Input data for polyethylene[a]

Unit-cell dimensions[b], $\boldsymbol{a}$	0.7640 nm
$\boldsymbol{b}$	0.4943 nm
Area per chain, $\boldsymbol{a}\cdot\boldsymbol{b}/2 = a_0 b_0$	0.1888 nm^2
Heat of fusion[b], Δh_f	2.8×10^9 erg cm^{-3}
Activation barrier[b], Q_D^*	2000 cal mol^{-1}
Fold surface free energy[b], $\sigma_{e(110)}$	90 erg cm^{-2}
	4890 cal mol^{-1}
Dissolution temperature, T_d	
n-tetradecanol[c]	133.5°C
n-hexadecane[c]	124.5°C
xylene[d]	110.5°C
Regime transition temperature, $T_{I\to II}$	
n-tetradecanol[e]	113.7°C, $\Delta T_{I\to II} = 19.8$°C
n-hexadecane[e]	102.1°C, $\Delta T_{I\to II} = 22.4$°C
Work of chain folding[b], q_{110}	4900 cal mol^{-1}
Serrated surface contact length, s	0.9101 nm
Stem widths, a_{110}	0.4550 nm
a_{200} (= $\boldsymbol{b}$)	0.4943 nm
Stem thicknesses, b_{110} (= d_{110})	0.4150 nm
b_{200} (= $\boldsymbol{a}/2$)	0.3820 nm

[a] 1 erg cm^{-3} = 0.1 J m^{-3}; 1 erg cm^{-2} = 1 mJ m^{-2}; 1 cal = 4.184 J
[b] Commonly accepted values[12,33]
[c] From T'_m *versus* $1/l$ plots[25]
[d] From T'_m *versus* $1/l$ plot[24]
[e] From ref. 25

Analysis of the {1 1 0} growth rate data of *Figures 4a* and *5a* follows a traditional path: a plot of $\ln G_{110} + Q_D^*/RT - \ln \Delta T$ *versus* $1/T\Delta T$ according to equation (23) yields a straight line for each regime whose slope is the appropriate $K_{g(i)}$ of equation (24) and whose intercept yields a value for the pre-exponential C_i of equation (23). The results of this analysis of the {1 1 0} growth rate data are listed in *Table 2*: only the values of $K_{g(I)}$ for regime I are included since the value of $K_{g(II)}$ is just one-half of $K_{g(I)}$, within 10%.

Analysis of the {2 0 0} data of *Figures 4b* and *5b* is slightly more complicated. From equation (12a), a plot of $\ln g_{200} + q_{200}/kT + Q_D^*/RT - \ln \Delta T_s$ *versus* $1/T\Delta T_s$ should yield a straight line with slope K_s. Such a plot, however, requires values of $\sigma_{e(200)}$, through equation (15), and of T_s, neither of which is available *a priori*. Accordingly, we proceeded in an iterative manner. To fit one of the curves for g_{200}, for example, we assumed a value of $\sigma_{e(200)}$ (hence, of q_{200}) and determined that value of σ_s (hence, T_s) that gave the 'best' linear least-squares fit of the data in the $1/T\Delta T_s$ plot based upon equation (12a). The slope of that line yielded a value for the nucleation constant which we label $K_{s(expt)}$. This process was repeated for other choices of $\sigma_{e(200)}$, each such choice yielding a separate value of $K_{s(expt)}$ for the appropriate value of σ_s. Values of $K_{s(expt)}$ thus obtained are plotted as a function of $\sigma_{e(200)}$ in *Figure 8* (lines denoted '1'). It can be seen that the value of $K_{s(expt)}$ is relatively insensitive to the choice of $\sigma_{e(200)}$ and is, therefore, reasonably accurately estabished by this means alone. For each $\sigma_{e(200)}$, σ_s pair, equation (14) was used to determine also a calculated value of the nucleation constant, $K_{s(calc)}$, which was found to vary almost linearly with choice of $\sigma_{e(200)}$ (*Figure 8*, lines denoted '2'). The final stage of the analysis, then, set $K_{s(expt)} = K_{s(calc)}$ which thereby gave the appropriate values of K_s (in this case, $K_{s(g)}$) and of $\sigma_{e(200)}$ and led directly to an appropriate value for σ_s based on the deduced value of $K_{s(g)}$. This process clearly established the intersection of the two lines in each part of *Figure 8* as the relevant solution. With values of $\sigma_{e(200)}$ and σ_s thus determined, the g_{200} and G_{200} data sets were analysed according to equations (12a) and (13), respectively, to yield the values of the parameters listed in the columns labelled 'from $g(T)$' in *Table 2*.

An analogous procedure was followed for the G_{200} data based on equation (13), regime II ($j=2$), in accord with criterion (c) above. This analysis yielded the values listed in the columns labelled 'from $G(T)$'.

Table 2 thus lists the results of our analysis of the growth rate data shown in *Figures 4* and *5* in terms of parameters appearing in equations (12)–(26). The upper portion of the table contains the results of a conventional flat-surface analysis of the growth of the dominant {1 1 0} sectors; the lower portion contains the results according to the expanded nucleation model involving lattice strain. Note that the values for $K_{s(g)}$ and $K_{s(G)}$ are in good agreement for a specified solvent and type of analysis and are not greatly different for the two solvents. Included in this table, insofar as was possible, is an

* 1 erg cm^{-2} = 1 mJ m^{-2}

Table 2 Results of 'strained crystal' analysis

(a) {1 1 0} sectors

Parameter	n-Tetradecanol	n-Hexadecane	Xylene
$K_{g(I)}$ (K^2)	0.9197×10^5	1.129×10^5	0.8848×10^5
C_I (cm s^{-1} K^{-1})	0.296	0.450	0.00488
C_{II} (cm s^{-1} K^{-1})	0.01725	0.01447	
$\sigma\sigma_e$ (erg^2 cm^{-4})	526.69	661.34	521.01
σ (erg cm^{-2}) (based on $\sigma_e = 90$)	5.85	7.35	5.79
$\sigma_{e(110)}$ (erg cm^{-2})[a]	78.0	98.5	89.7
σ (erg cm^{-2}) (based on $\sigma_{e(110)}$ in row above)	6.75	6.71	5.81
q_{110} (cal mol^{-1})	4250	5360	4880

(b) {2 0 0} sectors

	n-Tetradecanol		n-Hexadecane		
Parameter	From $g(T)$, eq. (12a)	From $G(T)$, eq. (13), $j = 2$	From $g(T)$, eq. (12a)	From $G(T)$, eq. (13), $j = 2$	Xylene
$\sigma_{e(200)}$ (erg cm^{-2})	81.9	75.6	(52.5)	65.8	62–118[b]
σ_s (erg cm^{-2})	1.24[c]	1.28	1.74[c]	1.66	0.9–1.3[d]
$\sigma_s\sigma_{e(200)}$ (erg^2 cm^{-4})	101	96.5	(91.1)	108	
T_s (°C)	124.8	124.6	112.6	113.2	
$K_{s(g)}$ (K^2)	1.94×10^4	1.80×10^4[e]	1.71×10^4	1.96×10^4[e]	
$g_{0(200)}$ (cm s^{-1} K^{-1})	0.101	0.0549[e]	0.00787	0.0292[e]	
$K_{s(G)}$ (K^2)	1.98×10^4[f]	1.85×10^4	1.78×10^4[f]	2.04×10^4	
$G_{0(200)}$ (cm s^{-1} K^{-1})	0.00249[f]	0.00169	0.000493[f]	0.00113	
q_{200} (cal mol^{-1})	4450	4110	(2850)	3570	
W_{200} (cal mol^{-1})[g]	7440	7200	7050	7580	
W_{200}/q_{110}[h]	1.52	1.47	1.44	1.55	>1[i]

[a] Values from ref. 24 (corrected)
[b] Range of values suggested in ref. 15
[c] For the 'square' lattice model[33], σ_s is 1.82 and 1.29 erg cm^{-2} for n-hexadecane and n-tetradecanol, respectively
[d] Based on molecular energy calculations[29] for representative core stem lengths of 10–15 nm
[e] Inferred from the fit of the g_{200} data to equation (12a) with values of $\sigma_{e(200)}$ and σ_s from analysis of the G_{200} data
[f] Inferred from the fit of the G_{200} data to equation (13) for $j = 2$ with values of $\sigma_{e(200)}$ and σ_s from analysis of the g_{200} data
[g] Calculated for a representative stem length of 18.5 nm
[h] With $q_{110} = 4900$ cal mol^{-1} corresponding to $\sigma_{e(110)} = 90$ erg cm^{-2}
[i] Estimate based on the observation that sector curvature in crystals grown from xylene is detected only at relatively low undercoolings[15]

analysis of data relevant to the crystallization of PE from dilute xylene solution (the data in *Figure 2*, primarily). Values of K_s and σ_s cannot be obtained at this juncture for crystals formed in xylene since no curvature could be detected within the temperature range where the growth rates are known. It may be possible in the future to obtain K_s and σ_s for the xylene case since it is known that curved edges do appear in crystals with high aspect ratios grown from this solvent at high growth temperatures[15].

For the {1 1 0} sectors, comparison of the values listed in the table with those accepted for the melt is in order. The value of the product $\sigma\sigma_e$ in solution is approximately one-half that found for the melt[12]. If the 'universal' value $\sigma_{e(110)} = 90$ erg cm^{-2} is adopted, σ values deduced for all three solvents (row 5) are smaller than the value $\sigma \simeq 11.8$ erg cm^{-2} appropriate for the melt[5] and the variation in the value of σ between the solvents is fairly marked, especially for n-hexadecane. For values of $\sigma_{e(110)}$ appropriate to the Organ–Keller analysis[24] (row 6), the variation of σ with solvent persists but is less marked (row 7). Either way, the evidence is clear that σ in dilute solution is lower than it is in the melt. It would be of interest to have a detailed theoretical explanation of why σ is lower in the presence of solvent. Of importance here is that our analysis in terms of lattice strain and its significance is not affected by the existence of the low values of σ in the case of crystallization from dilute solution. While there is some uncertainty about the absolute value of σ appropriate to each solvent, the growth of the {1 1 0} sectors in solution appears to be well represented by the conventional LH approach, including the fact that $K_{g(I)} \simeq 2K_{g(II)}$ as required by regime theory.

It is instructive to note the similarities in the behaviour of solution-grown crystals of PE and melt-crystallized fractions. In the latter[5,12], a dominant {1 1 0} growth front controls the kinetics of growth of the spherulites and axialities and a regime I → II transition is clearly present: the front is of the 'flat-surface' type with no significant lattice strain effects. The behaviour of $G_{110(tip)}$ in a solution-grown crystal is analogous to this with respect both to the presence of the I → II transition*

* The undercooling at the I → II regime transition $\Delta T_{I\to II}$ is 16.5 ± 0.5 K for the melt[5] and is only slightly larger in the presence of solvent – see *Table 1*

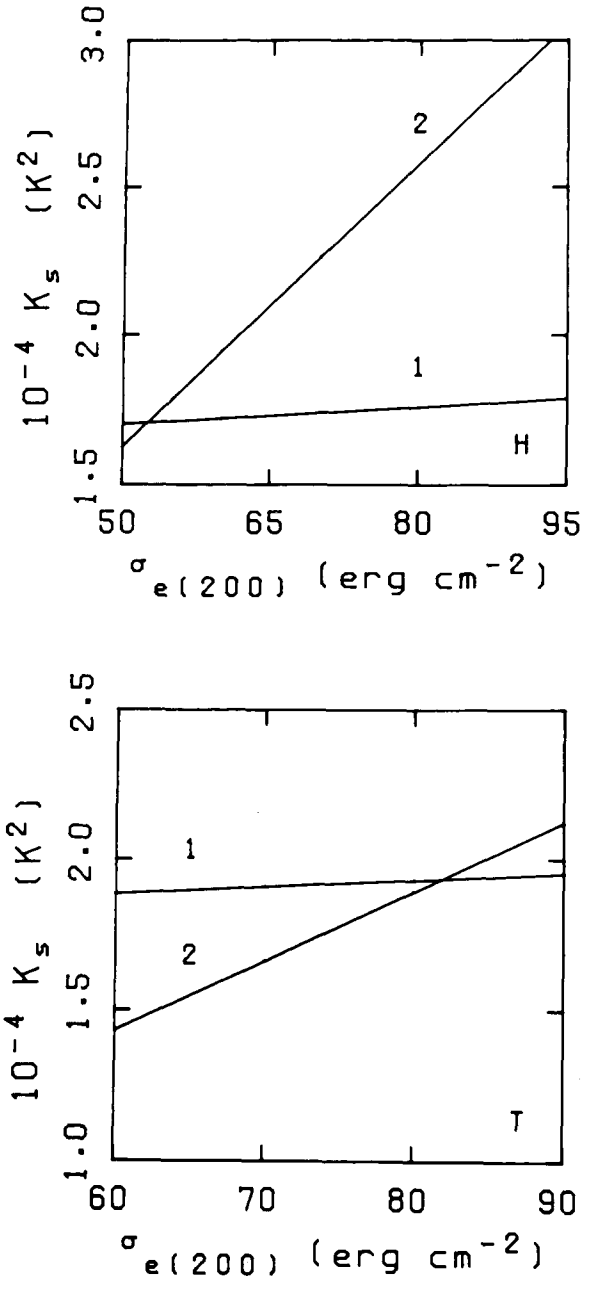

Figure 8 Lattice strain nucleation constant K_s as a function of choice of $\sigma_{e(200)}$. 1, K_s as evaluated from g_{200} (equation (12)) by least-squares fit; 2, K_s as calculated from K_s from equation (14). The intersection of the two lines establishes the 'best' value of $\sigma_{e(200)}$ and of σ_s. Upper part (H), n-hexadecane; lower part (T), n-tetradecanol. (The corresponding plot for n-hexadecane based on G_{200} gives an intersection at $\sigma_{e(200)} = 65.8$ erg cm^{-2})

(*Figure 2*) and to the applicability of the 'flat-surface' model. With the {1 1 0} growth faces being dominant, the direction of maximum growth rate is naturally collinear with the ***b*** direction of the unit cell in each case. Further, there is evidence of lattice strain in the {2 0 0} regions of both melt- and solution-grown crystals. In melt-crystallized PE, the lattice expansion is mainly along the ***a*** direction of the unit cell[28]. This is reasonably attributed to repulsion of the {2 0 0} folds. In the present treatment of solution-grown crystals in terms of the 'serrated-surface' model for a {2 0 0} sector, the presence of lattice strain effects resulting from repulsions in the {2 0 0} fold array is clearly evident.

We now show that growth of the {2 0 0} sectors is consistent with regime II. This is readily demonstrated using the familiar Lauritzen 'Z_L' test[9], where Z_L is a number defined as:

$$Z_L = iL^2/4g \tag{27a}$$

in which i is the nucleation rate, g the substrate completion rate and L the substrate length. If $Z_L \leqslant 0.1$, the system is in regime I and if $Z_L \geqslant 1$, the system is in regime II; the regime I → II transition occurs at $Z_L \sim 1/2$.

Consider the {2 0 0} serrated face with lattice strain as exemplified by the behaviour of $G_{200}(T)$. Suppose that regime II is appropriate, as assumed in the Mansfield relations. The general regime II definition is $G_{II} = b_0(2ig)^{1/2}$. With g_{200} and i_{200} given by equations (12) and G_{200} of equation (13) taken to be in regime II ($j = 2$), it is found that the Z_L test is to be made with:

$$Z_{L(200)} = \frac{L^2}{4}\left(\frac{i_{0(200)}}{g_{0(200)}}\right)\exp\left(\frac{q_{200}}{kT}\right)$$
$$= \frac{1}{2}\left(\frac{L}{2b_0}\right)^2\left(\frac{G_{0(200)}}{g_{0(200)}}\right)^2\exp\left(\frac{q_{200}}{kT}\right) \tag{27b}$$

(regime II assumed)

where $G_{0(200)}$ is understood to be the pre-exponential factor for regime II (i.e. $j = 2$), as listed in *Table 2*. Except for L, the second equality in equation (27b) involves directly observed quantities. Relevant values of $g_{0(200)}$ derived from experiment are listed in *Table 2*. It is readily shown with the effective value of L being $2ht$ that $Z_{L(200)} \gg 1$, which is consistent with regime II behaviour. The result $Z_{L(200)} > 1$ holds even for a crystal where $2ht$ is as small as 10 nm. Accordingly, the assignment of growth on the {2 0 0} face as regime II is self-consistent with respect to the derivation of the Mansfield relations via criterion (c) above, the Lauritzen 'Z_L' test and the kinetics based on the 'serrated' model with lattice strain. This holds irrespective of the regime active on the {1 1 0} face. Furthermore, when properly plotted with ΔT_s as the undercooling scale in $1/T\Delta T_s$, the experimental ln G_{200} data, which do not depend on the Mansfield relations, show no evidence of a normal I → II regime transition with the correct slope ratio for any reasonable value of σ_s. The assumption $\sigma_s \simeq 0$, giving $\Delta T_s \simeq \Delta T$, does lead to an 'apparent' I → II transition, but this assumption cannot be justified because of the undeniable presence of significant lattice strain in the {2 0 0} sectors. In summary, the behaviour of growth on the {2 0 0} face is consistent with its being regime II over the entire experimental range. With a definite regime I → II transition being known to occur on the {1 1 0} front, it follows that a regime transition can appear on one face of a growing crystal of this type and not on the other. Regime II persists on the {2 0 0} faces largely because the effective substrate length is much larger and the substrate completion rate much smaller for the 'serrated' model with lattice strain as compared with these same quantities for the conventional flat-surface model (cf. equation (27a)).*

* The extremely slow substrate completion rate on the {2 0 0} face evidently allows time for stem addition to bypass the defects that would otherwise define an effective L on a shorter timescale, thereby leading to multiple nucleation and regime II behaviour on that face (criterion (c)). A parallel argument has been employed to explain examples of the re-emergence of regime II at growth temperatures *above* regime I (ref. 26 and references therein)

DISCUSSION

Mansfield[31,32] provided the means whereby the characteristics of lamellae with curved edges could be analysed in terms of the rates of substrate completion and of crystal growth. The lattice strain model described above permits expressions for these same rates to be understood in detail with a straightforward extension of nucleation theory. In addition, the lattice strain model with a serrated growth face unexpectedly predicted the existence of a maximum temperature in each solvent at which curved-edge crystals could be grown—see later. It is significant that the introduction of only one additional parameter, σ_s, essentially uniquely determined, permitted the Organ–Keller data on solution-grown single crystals of PE to be analysed in detail. Values of the lattice strain parameter σ_s deduced and listed in *Table 2* are in reasonable agreement with the value estimated from molecular energy calculations by Marand[29] (see *Table 2*). Recall that there is direct and independent evidence of strain in the {2 0 0} sectors[28]. The {2 0 0} sector clearly *is* different from the {1 1 0} in that it possesses significant lattice strain, requiring that σ_s (and consequently T_s) be introduced into the theory, and it has the energetic characteristics of a serrated rather than a flat growth front, such that virtually no additional σ-type surface is involved in the nucleation act.

There are additional criteria that must be met in these crystals. One of these is the match of stem lengths at the sector boundaries. Wittmann and Lotz[30] and Khoury[40] have indicated that no discontinuity in lamellar thickness exists at sector boundaries, but this does not necessarily require that lamellar thicknesses be exactly the same in the body of the {1 1 0} and {2 0 0} sectors. Since the expressions for the stem lengths in the two sectors, equations (11) and (21), while of the same general form, have different functionalities, it follows that the degree of tilt in the body of adjoining sectors will be different unless the lamellar thicknesses are quite different in the two types of sector. Following an analysis scheme adopted earlier[41] for lamellar thickness data, we show in *Figure 9* illustrative calculations of the stem lengths for the two sectors. (The larger δ_{200} as compared with δ_{110} contributes significantly to $l^*_{g(200)}$ being larger than $l^*_{g(110)}$.) The calculated curves agree reasonably well at the lower crystallization temperatures. Higher temperatures require progressively increasing angles of tilt in the {2 0 0} sectors (relative to that in the {1 1 0} sectors), which are not excessive for PE. The exact details of the calculation of the stem lengths depends strongly on the value of $\sigma_{e(110)}$ chosen, and our results should be regarded as being illustrative rather than strictly quantitative. For *Figure 9*, we have used the value 90 erg cm^{-2} and other relevant parameters from *Table 1*. Observe that l^*_g is correctly to be identified with the stem length in this situation and not with the lamellar thickness. In support of the calculations shown in *Figure 9*, Runt *et al.*[42], from longitudinal acoustic mode (LAM) studies of PE single crystals, established that the stem lengths were greater in the {2 0 0} than in the {1 1 0} sectors. This result is consistent with the theoretical prediction of the present model.

Rough estimates of the angle of tilt in the {2 0 0} sectors can be given based upon the results in *Figure 9*. For simplicity, we take the stems in the {1 1 0} sectors to be normal to the fold planes. For n-hexadecane (upper figure) the tilt angle in the {2 0 0} sectors would vary

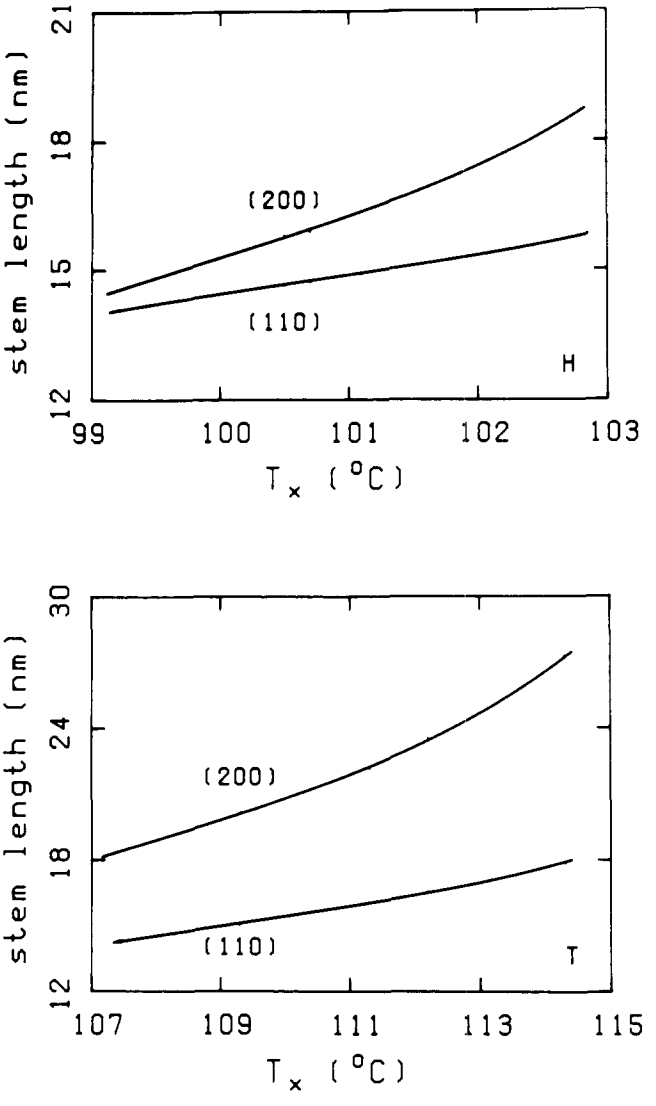

Figure 9 Calculated l^*_g curves for {1 1 0} and {2 0 0} sectors. Upper part (H), 0.05% in n-hexadecane; lower part (T), 0.05% in n-tetradecanol. These results apply to the body (and growth front) of the designated sector

from 14.4 to 32.5° for the temperature range shown (with an angle of 49.2° at the highest reported crystallization temperature). For n-tetradecanol (lower figure) the corresponding range of tilt angles would be 39.1 to 49.0° for the range depicted (60.2° at the maximum crystallization temperature). Except possibly for n-tetradecanol at the highest growth temperature reported, tilt angles with these values are within an acceptable range and are not in disagreement with the angles deduced by Bassett and Hodges[43] in lamellae extracted from melt-crystallized PE (mean tilt angles of 30 and 40° with a variation around each mean of ±15°). Also, LaBaig[17] found a tilt angle of −45° in melt-crystallized specimens. The foregoing suggests that lamellar thicknesses in the body of the two types of sectors are rather similar so that the different stem lengths in these sectors do in fact cause different angles of tilt rather than considerably different lamellar thicknesses. There must be notable changes of tilt in the immediate vicinity of the sector boundaries since the lamellar thicknesses are essentially the same there, but with the stem lengths wishing to be different. This is probably connected with the fact that varying angles of tilt are seen presumably

within a given sector[40,44]. Our approximate estimates of tilt refer to the body of the {2 0 0} sector (including the growth front) and do not attempt to explain precise details of what occurs exactly at and very near sector boundaries.

From the results listed in *Table 2* it is seen that the work to form an isolated {2 0 0} chain fold, q_{200}, can be significantly less than that of forming a {1 1 0} fold. This agrees with the semiempirical molecular energy calculations by Davé and Farmer[34] and by others cited therein. However, the *total* work of forming the chain fold and placing it, with its stem, on the lamellar surface, W_{200} in equation (16), is greater than that for the {1 1 0} fold because it includes the term, $sl\sigma_s$, arising from the lattice expansion caused by chain fold repulsions—the lattice strain free energy. As a consequence, it requires approximately one and a half times as much work to form a unit of area (say, that corresponding to one stem) for the folded {2 0 0} sectors as for the {1 1 0} ones. The increased work is sufficient to make the {2 0 0} sectors subordinate to the {1 1 0} sectors in terms of growth rate but not so large as to make growth of the {2 0 0} sectors impossible nor to cause the elimination of the {2 0 0} sectors in the crystals. Even though the values deduced for $\sigma_{e(200)}$ and σ_s in the two solvents are rather different, their combination in the total work of chain folding, W_{200}, compensates to yield a reasonably constant value for the {2 0 0} sectors (*Table 2*). It is safe to conclude that the overall work of forming a {2 0 0}-type surface involving both stems and chain folds and including lattice strain effects induced by fold repulsions is $\sim 7400 \pm 350$ cal mol^{-1} as compared with ~ 4900 cal mol^{-1} (based on $\sigma_{e(110)} = 90$ erg cm^{-2}) for the corresponding process for a {1 1 0}-type surface.

An adjunct of the analysis with the lattice strain model is the prediction that a strained {2 0 0} sector should melt at a lower temperature than will an adjacent {1 1 0} sector. From equations (22) and (17), the exact formula for the temperature difference with solution present is:

$$T'_{d(110)} - T'_{d(200)} = \frac{2T_d}{\Delta h_f}\left(\frac{\sigma_{e(200)}}{l_{200}} - \frac{\sigma_{e(110)}}{l_{110}} + \frac{s\sigma_s}{2a_0b_0}\right) \quad (28)$$

where one may set $l = l_{200} \simeq l_{110}$ for obtaining rough estimates.

With l assumed to be 18.5 nm and $\sigma_{e(110)} = 90$ erg cm^{-2} (and values of the other parameters from the tables), estimates of the temperature differences using equation (28) are in the vicinity of 6.1 and 7.4°C for n-hexadecane and n-tetradecanol, respectively. These estimates assume that no annealing (thickening or other process that might relieve strain) takes place during the crystallization process or during the melting run, this being a particularly hazardous assumption in view of the rather high temperatures involved. Thus, the σ_s effect at the growth front that controls the kinetics, and which in turn leads to highly accurate predictions of the shape as a function of growth temperature (see later), may in some cases be partially erased in the main body of the crystal by annealing processes. Accordingly, the temperature differences cited above should be taken as upper bounds of an illustrative character. We also note that, in the general case, σ_s may decrease with increasing stem length[29,33] with the end result that $T'_{m(110)} - T'_{m(200)}$ may be expected to decrease somewhat with increasing crystallization temperature and axial ratio if a sufficient temperature range is involved. That there can be different melting points in different sectors is supported by observations on the truncated, non-curved-edge PE crystals grown from dilute xylene solution by Bassett *et al.*[45,46], by Harrison[47,48] and by Alfonso *et al.*[36]. Also, Organ and Keller[49] detected a clear melting-point difference of the predicted type in PE crystals with a low axial ratio that were dispersed in silicone oil. This difference did not appear in crystals with higher axial ratios that were formed at higher temperatures, perhaps because of annealing effects, which were known to be present. One may conclude from the cited references, taken in sum, that when there is a melting-point difference, the {2 0 0} sectors generally melt out first, in qualitative agreement with our predictions.

As mentioned previously, if one has values of G_{110}, G_{200} and g_{200} one may solve the parametric equation (5) to obtain a value of h and, hence, A_r and C. Since *Table 2* contains values of the constants in the growth rate equations (12a), (13) with $j = 2$, and (18) for a {2 0 0} curved edge and (23) with $j = 1$ and 2 for a {1 1 0} face for the two solvents, we were able to calculate the shape of the PE crystals expected as a function of crystallization temperature. Representative examples are shown in *Figures 10* and *11* for the limits of the experimental temperature range reported by Organ and Keller[25] for each solvent and, in *Figure 10*, for the

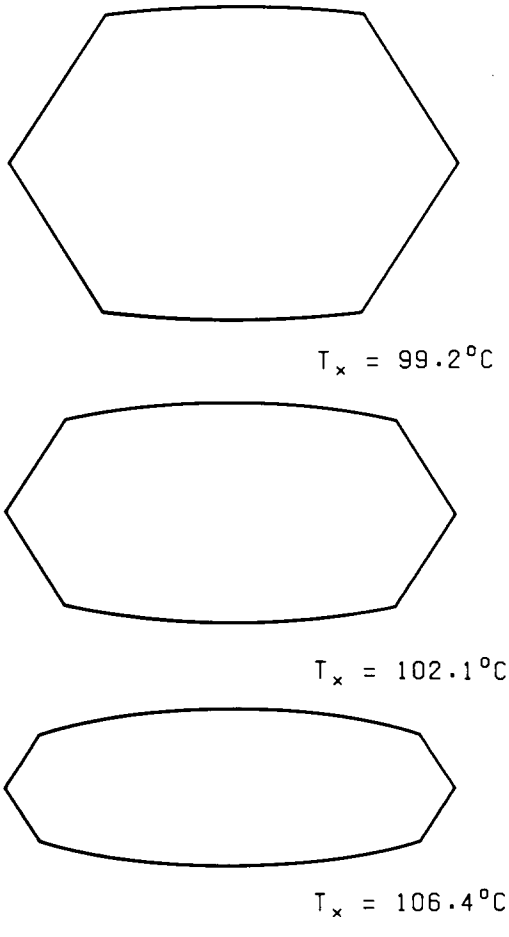

Figure 10 The shape of polyethylene single crystals grown in n-hexadecane at various crystallization temperatures calculated according to the lattice strain model with serrated surface using values of the parameters from *Table 2*. The extremes shown represent the limits of the experimental data of Organ and Keller[25]

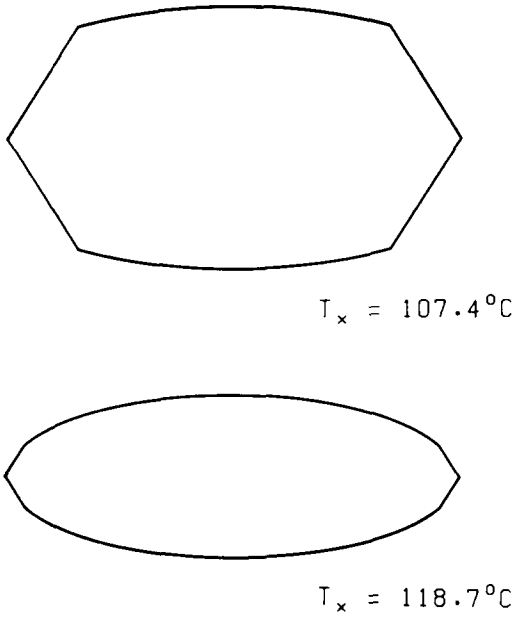

Figure 11 As in *Figure 10* but for n-tetradecanol

regime I → II transition temperature in n-hexadecane. Note that the calculated shapes are based on the results of a *nucleation theory* analysis! It is clear that these agree well with the Organ and Keller shape data (*Figure 3*) throughout the entire experimental range for both solvents. The curved edge is predicted to be a section of an ellipse[31] and this accords well with electron micrographs in the literature.*

The growth rate equations evaluated here may be used together with the Mansfield phenomenological relations to extrapolate shape behaviour to temperatures outside of the experimental temperature range. From the behaviour of the data shown in *Figure 2*, one might well expect PE lamellae with curved edges to grow readily (if slowly) at temperatures well above those reported. However, extrapolation of our calculations to temperatures closely proximate to or only slightly higher than those reported by Organ and Keller was impossible: the critical parameter h/g_{200} exceeded unity essentially at the highest growth temperature experimentally reported for each solvent and the solution of the shape equations became imaginary. Thus, we postulate that the highest temperature reported may well be close to the highest temperature of growth possible for the type of crystal in *Figure 1* for each system, that is, that $T_{max(expt)} \simeq T_{max(calc)}$. For n-hexadecane, the experimental and calculated values are 106.4 *versus* 106.75°C; and for n-tetradecanol, the values are 118.8 *versus* 118.73°C, respectively.

Recent unpublished experiments carried out at the University of Bristol[50] indicate that an upper temperature limit for growth of the type of crystal depicted in *Figure 1* may well exist. The same whole polymer PE and solvents discussed here were employed (because of the polydispersity of the sample, fractionation effects occurred). It was estimated that formation of this type of crystal would cease ~2°C above $T_{max(calc)}$ for each solvent. We interpret these observations to mean that a T_{max} effect was present. Provided this interpretation is correct, it would lend strong support to both the model and the analysis given here. From a theoretical viewpoint, the cessation of growth of this type of crystal near $T_{max(calc)}$ can be traced back to the repulsion of {2 0 0} chain folds. This repulsion induces significant lattice strain as embodied in σ_s which, in turn, simply stops nucleation and substrate completion in the {2 0 0} sector at T_{max}. This cut-off effect at a specific high growth temperature also correlates with the increasing difference in stem lengths (hence, tilt) in the two sectors with increasing growth temperature. The difference in tilt angle also can be traced through σ_s back to the repulsion of chain folds in the {2 0 0} sectors, this effect being absent or minimal in the {1 1 0} sectors.

Extrapolation to lower crystallization temperatures is also readily possible for both solvent systems. Empirically, extrapolation of the deduced θ values (not shown) or of the curvature data of *Figure 3* suggests that θ and/or C should vanish at approximately 90°C (the least-squares broken line shown in *Figure 3b* has a correlation coefficient of 0.97). On this basis, crystals with curved edges would not be expected at or below 90°C for crystallization from dilute solution for the solvents noted.

It is found that this empirical prediction, though possibly leading to a correct result, may be misleading. The *calculated* shape changes with decreasing crystallization temperature based on parameter values listed in *Table 2* are different from those expected based upon simple extrapolation from within the experimental range (*Figure 3*). The calculations (which are of the same type used to produce *Figures 10* and *11*) indicate a small cusp in the aspect ratio and the curvature at the {1 1 0} regime I → II transition (which would be smoothed because of the slightly diffuse nature of the regime transition) and an *increase* in both curvature and aspect ratio with decreasing temperature starting at a temperature some 5–10°C below the reported minimum experimental temperature. No experimental observations in this temperature range have been reported for the two solvents. However, we surmise that regime III crystallization[11] may begin on the {1 1 0} faces in the low-temperature range. If such is the case, the solution of the shape equations becomes imaginary for temperatures more than a few degrees below the temperature at which the regime II → III transition might be expected to intervene, which should correspond to $\Delta T_{II \to III} \sim$ 30–35°C. Thus, with regime III assumed, there is a temperature, T_{min}, below which one does not expect crystals of the general type depicted in *Figure 1* to form. (Presumably, below T_{min}, diamond-shaped lozenge single crystals, or perhaps dendritic crystals, with all {1 1 0} sectors, would be formed.) Experimentation at lower crystallization temperatures is clearly desirable for PE in the solvents considered here particularly to determine if a regime II → III transition and a corresponding morphological change does indeed occur. The overall situation, then, is that crystals of the general type illustrated in *Figure 1* are predicted to occur only within a restricted temperature range bounded by T_{min} and T_{max}.

As reported in *Table 2*, the work W_{200} to form and

* With only a small change in the input data, lenticular crystals representing the extreme form of that depicted in *Figure 11* for the higher temperature, i.e. crystals that have only very small {1 1 0} faces and long elliptical {2 0 0} edges, can be accounted for. While such do not appear in the Organ–Keller studies, objects apparently of this type have been extracted by Keith *et al.* and Bassett *et al.*[17] from melt-crystallized PE grown at high temperatures in regime I. At the opposite extreme, Professor M. L. Mansfield of MMI has pointed out to the authors that nearly circular crystals can arise under the condition $G_{200} \simeq g_{200}$ for a 'square lattice' model. See Note added in proof

pack a fold with the concomitant lattice expansion in the {2 0 0} sector is greater than the corresponding process in an unstrained {1 1 0} sector (cf. the W_{200}/q_{110} values in the last row). One may infer from the schematic diagram of *Figure 7* that the fold packing problem could lead to a greater degree of non-adjacency and/or tilt within the {2 0 0} sectors. (In this connection, Mansfield[51] and Kumar and Yoon[52] have shown that a higher work of chain folding, interpreted here to mean W_{200}, reduces the tendency for adjacent re-entry.) This reduced preference for strict adjacency will tend to give rise to a 'fold' surface of a more disordered type than appears for {1 1 0}. We consider these factors to be the probable cause of the somewhat more disorganized appearance[30] reported for 'decorated' {2 0 0} fold surfaces as compared with the {1 1 0}. We recognize, of course, that the appearance of a 'decorated' surface provides only a highly qualitative measure of the nature of the underlying structure. Consideration of the ability to form {2 0 0} folds and of their shape has been given by Patel and Farmer[53] (and references cited therein) and by Davé and Farmer[34]. Recall that the latter authors predict repulsion of {2 0 0} chain folds.

It is proper to ask why a strained flat-surface model, analogous to that used for the dominant {1 1 0} growth front, would not be relevant to {2 0 0} growth as well. The answer is straightforward: in the derivation of the flux-based equations for such a model, the lattice strain parameter σ_s appears as $(\sigma + \sigma_s/2)\sigma_e$ in the nucleation parameter K_g in 'G_{200}' $\propto \exp(-K_g/T\Delta T_s)$, whereas '$g_{200}$' $\propto \exp[-2(a_0 + b_0)\sigma_s\sigma_e/\Delta G_s kT]$[33]. Hence, '$G_{200}$' and '$g_{200}$' would no longer have the same temperature dependence (would no longer be parallel) and the {2 0 0} growth faces would be expected to exhibit (in principle) a regime transition. Each of these expectations would violate a constraint enumerated above and each, therefore, invalidates a flat-surface model for the curved edge. Further details are given in a previous publication[33].

The effect of the strain might be expected to decrease with increasing lamellar thickness, i.e. with increasing crystallization temperature[33]. In this vein, the X-ray studies of Davis *et al.*[28] can be interpreted to indicate that the thicker the lamella the less important the fold repulsion effects in the interior lattice. Also, Marand's calculations[29] exhibit a decrease of σ_s with increasing l. It was found in the course of the present analysis that σ_s does indeed decrease slightly with increasing crystallization temperature (i.e. with increasing lamellar thickness). This effect is small but can be detected in the results from the analysis of the more extensive data for n-tetradecanol.

In addition to the previously known concentration effect[19,54,55], the solvent clearly affects the surface energetics of the crystals grown. This is most clear in the case of σ, which relates only to the {1 1 0} sectors. Whatever route is employed to evaluate it, σ is definitely lower in the solution case (5.8–7.4 erg cm^{-2}) than for the melt ($\sim$12 erg cm^{-2}). In the case of the {2 0 0} sectors the most notable apparent solvent effect involves σ_s. The higher σ_s found for n-hexadecane, however, may result from the fact that the {2 0 0} sectors in the crystals formed in this solvent are thinner in the accessible experimental range than those formed in n-tetradecanol (cf. *Figure 9*). Further, even if one ignores the surprisingly low values of $\sigma_{e(200)}$ and q_{200} for n-hexadecane (*Table 2*, column 'from $g(T)$'), these quantities still appear to be lower for this solvent. However, though the {2 0 0} sector surface free energies for PE in the two solvents are seemingly different, the total work of forming a fold plus stem in a chain-folded {2 0 0} sector, W_{200}, is nearly the same for the two solvents. Evidently the solvent to some extent controls the balance between fold surface energy $\sigma_{e(200)}$ and lattice strain as described by σ_s in such a way as to maintain the product $\sigma_s\sigma_{e(200)}$ and the total work of chain folding W_{200} essentially constant.

It is conceivable that the asymmetric, curved lamellar structures observed by Keith *et al.*[17] in crystals of PE may be amenable to an extension of the type of model presented here. These crystals were grown from the melt at the relatively high temperatures corresponding to regime I for the {1 1 0} sectors, and the habits observed involved chain tilt angles of up to 45°. DiCorleto and Bassett[56], from anabaric PE sample preparations from the melt, have extracted lamellae that are circular discs which were formed in the hexagonal, rather than in the orthorhombic, phase. Our model of curved-edge crystals presented here may not be applicable directly to crystals with such higher symmetry. However, an analysis of such crystals might be attempted under the assumption that the growth front of the hexagonal phase is both strained and serrated. One notes that even in the extended-chain crystals of n-paraffins strain effects appear[28], the repulsion of CH_3– end-groups being far smaller than that of {2 0 0} sector chain folds. Accordingly, curved-edge crystals of the origin suggested here, such as appear near the melting point in n-$C_{94}H_{190}$ (ref. 57),* are not necessarily excluded from consideration.

Finally, we comment on the sensitivity of our analysis to choice of key input parameters. In particular, we must consider the effect of the value of $\sigma_{e(110)}$ used on the results obtained. As indicated in *Table 2* and in the discussion above, Organ and Keller found a considerable variation among different solvents but others did not. We thus chose the value $\sigma_{e(110)} = 90$ erg cm^{-2} for the principal analysis. Most of the results listed in *Table 2* are unaffected by the value chosen for $\sigma_{e(110)}$. Its effect is seen first in the value of σ deduced from analysis of growth rate data (G_{110}), which affects only the calculation of {1 1 0} stem lengths (and comparisons, such as in *Figure 9*). Second, it affects slightly the comparison of the work of chain folding (W_{200}/q_{110} row in *Table 2*). Consequently, except for this relatively minor uncertainty, our analysis of the data for curved-edge crystals of polyethylene, particularly in terms of the characteristics of the {2 0 0} sectors, is unaffected.

Another source of error could be in the value of the dissolution temperature, T_d, which affects the values of $K_{g(I)}$ and $K_{g(II)}$ and the ratio of the K_g values for the {1 1 0} faces. The T_d values employed here were based on T_m' *versus* $1/l$ plots[24,25], an accepted and potentially accurate method to obtain this quantity. An indication that the T_d values are essentially correct is that the ratio $K_{g(I)}/K_{g(II)}$ is 2 within 10% for both solvents. If T_d were seriously in error, this ratio would fall well outside this limit.

CONCLUSIONS

It is evident that nucleation theory, suitably expanded

* Crystals resembling in overall shape that depicted in *Figure 11* at $T_x = 118.7$°C are seen in highly purified n-$C_{94}H_{190}$ at very low undercoolings

and modified, can account in detail for the existence of lamellae with curved edges. For the case of PE single crystals, growth of the dominant {1 1 0} sectors follows the energetics associated with the classical LH theory for the model of a flat growth front without significant lattice strain. This model features a large 'σ' term so that growth in a given regime is according to $G_{110} \propto \exp(-K_g/T\Delta T)$, where K_g contains the factor $\sigma\sigma_{e(110)}$. Growth of the subordinate {2 0 0} sectors conforms to a new model in which there is no σ factor because of the serrated growth front and where the effect of lattice strain resulting from the repulsion of the {2 0 0} folds is taken into account through the lattice strain parameter σ_s; the result is that $G_{200} \propto \exp(-K_s/T\Delta T_s)$, where K_s contains the factor $\sigma_s\sigma_{e(200)}$ and where $\sigma_s < \sigma$. The substrate completion rate for the serrated and strained {2 0 0} face is reduced by an extra factor also involving K_s as in $g_{200} \propto \exp(-K_s/T\Delta T_s)$. Thus, in a bounded temperature range, g_{200} can become just slightly faster than the rate of advance of the crystal edge, which is closely equivalent to the growth rate of the {1 1 0} growth face. This is precisely the condition under which curvature conforming to the shape of a section of an ellipse will appear on the subordinate {2 0 0} growth face. The lattice strain reduces the stability of the {2 0 0} sector, with the result that the undercooling ΔT_s effective at the {2 0 0} growth front is smaller than that at {1 1 0}.

With the lattice strain model a single additional parameter whose existence is independently supportable, namely σ_s, permits one to: (1) fit aspect ratio and curvature data quantitatively over a considerable range of growth temperatures for two different solvents; (2) deduce values of σ_s and of the fold surface free energy of the strained sector; (3) explain the phenomenological behaviour of the growth rates, including the presence of regimes I and II on the {1 1 0} faces and the absence of the corresponding regime change on the {2 0 0} faces; (4) anticipate the poorer fold surface regularity and the larger angle of tilt in the {2 0 0} sectors; (5) explain (at least qualitatively) the lower melting point observed in the {2 0 0} sectors of certain 'truncated' crystals; (6) introduce a more sophisticated view of the *total* work of chain folding, involving both the work of forming the fold and the work of packing such a fold onto the surface of a lamella; (7) make use of the expanded definition of the total work of chain folding W_{200} to explain why growth in the {2 0 0} sectors is slower than it is in the {1 1 0} sectors, thus providing a rationale for '***b***' axis growth in PE (which has been a long-standing puzzle in polymer crystallization); (8) predict, apparently correctly, that there is an upper temperature limit, T_{max}, above which *Figure 1* type crystals cannot form; (9) predict the existence of an experimental lower crystallization temperature limit for the type of crystal considered; and (10) gain additional insight into the subtleties of polymer crystal growth, such as drawing attention to the effect of chain fold repulsions on growth rates and morphology. It is worth emphasizing that item (1) above can be stated another way: given σ_s and the normal input data, one can accurately predict detailed crystal shapes as a function of growth temperature for both solvents.

The lattice strain model with a molecularly serrated growth front appears reasonable on the basis of the known crystal structure and the inferred strain values have acceptable magnitudes. In particular, the general level of strain in the {2 0 0} sectors deduced here from the edge curvature is supported by independent evidence, namely by an estimate of the value of σ_s based upon the X-ray data (giving the degree of strain) combined with molecular energy calculations. It is evident that the LH flux equation version of nucleation theory remains a valid approach to polymer crystal growth with chain folding.

Further work is indicated. In order to achieve a better understanding of melting behaviour, it would be of interest to obtain melting-point data on PE crystals containing the two sector types under conditions where it was relatively certain that annealing effects were absent during both the crystallization and melting runs and where the lattice parameters indicating the degree of strain were known beforehand. Studies of the type executed by Organ and Keller but with different solvents are desirable to determine if the 'anomalous' behaviour of n-hexadecane with its apparently low $\sigma_{e(200)}$ and relatively large σ_s values is more general. Experiments with good PE fractions would be most useful in confirming (or refuting) the existence of the T_{max} effect. On general grounds it would be of interest to pursue the search for regime I → II transitions for PE in different solvents, including xylene, and to attempt to locate the regime II → III transition that is predicted to occur at large undercoolings in these solvents. From the theoretical viewpoint, it would be desirable to understand in detail why σ in the presence of solvent appears to be less than it is in the melt. Also, the curvature theory may need to be extended in order to apply to the novel lamellae derived from melt-crystallized PE by both Bassett *et al.* (circular lamellae from the hexagonal phase and lenticular crystals from the orthorhombic form) and by Keith *et al.* (asymmetric lamellae exhibiting curved edges). Finally, we acknowledge the theoretical challenges involved in adapting the theory to systems other than polyethylene.

ACKNOWLEDGEMENTS

We are grateful to Dr F. Khoury of NIST for many helpful discussions concerning details of crystals with curved edges and to Professor M. L. Mansfield of MMI for sharing the results of his analysis with us prior to its publication and for his contributions during the preparation of this work. Special thanks are due to Dr Sally J. Organ of the University of Bristol for executing the experiments on the upper temperature limit of crystal growth and providing the authors with the results, and to Professor A. Toda of Kyoto University for illuminating discussions concerning his alternate solution to the Frank equations. We also thank our many colleagues for their most useful comments on an earlier version of this work. One of the authors (JDH) gratefully acknowledges partial support of this research under Grant DMR 86-96049 of the National Science Foundation.

REFERENCES

1 Lauritzen, J. I. Jr and Hoffman, J. D. *J. Res. Natl. Bur. Stand. (A)* 1960, **64**, 73; Hoffman, J. D. and Lauritzen, J. I. Jr *J. Res. Natl. Bur. Stand. (A)* 1961, **65**, 297
2 Frank, F. C. and Tosi, M. *Proc. R. Soc. Lond. (A)* 1961, **263**, 323
3 Lauritzen, J. I. Jr and Passaglia, E. *J. Res. Natl. Bur. Stand. (A)* 1967, **71**, 261
4 Hoffman, J. D. *Polymer* 1982, **23**, 656
5 Hoffman, J. D. and Miller, R. L. *Macromolecules* 1988, **21**, 3038

6 Hoffman, J. D. and Weeks, J. J. *J. Res. Natl. Bur. Stand.* (*A*) 1962, **66**, 13
7 Hoffman, J. D. *Macromolecules* 1986, **19**, 1124
8 Lauritzen, J. I. Jr and Hoffman, J. D. *J. Appl. Phys.* 1973, **44**, 4340; Hoffman, J. D., Frolen, L. J., Ross, G. S. and Lauritzen, J. I. Jr *J. Res. Natl. Bur. Stand.* (*A*) 1975, **79**, 671
9 Lauritzen, J. I. Jr *J. Appl. Phys.* 1973, **44**, 4353
10 Frank, F. C. *J. Cryst. Growth* 1974, **22**, 233
11 Hoffman, J. D. *Polymer* 1983, **24**, 3
12 Hoffman, J. D., Davis, G. T. and Lauritzen, J. I. Jr in 'Treatise on Solid State Chemistry' (Ed. N. B. Hannay), Plenum Press, New York, 1976, Vol. 3, Ch. 7
13 Miller, R. L. in 'Flow-Induced Crystallization' (Ed. R. L. Miller), Gordon and Breach, New York, 1979, p. 31
14 Valenti, B. and Pedemonte, E. *Chim. Ind.* (*Milan*) 1972, **54**, 112
15 Passaglia, E. and Khoury, F. *Polymer* 1984, **25**, 631
16 Passaglia, E. and DiMarzio, E. A. *Polymer* 1986, **27**, 510
17 Keith, H. D. *J. Appl. Phys.* 1964, **35**, 3115; LaBaig, J. J. Doctoral Dissertation, Strasbourg, 1978; Keith, H. D., Padden, F. J. Jr, Lotz, B. and Wittmann, J. C. *Macromolecules* 1989, **22**, 2230; Bassett, D. C., Olley, R. H. and Al Raheil, I. A. M. *Polymer* 1988, **29**, 1539
18 Toda, A. *J. Phys. Soc. Japan* 1986, **55**, 3419
19 Toda, A. *Polymer* 1987, **28**, 1645
20 Sadler, D. M. *Polymer* 1987, **28**, 1440 and references therein
21 Holland, V. F., Mitchell, S. B., Hunter, W. L. and Lindenmeyer, P. H. *J. Polym. Sci.* 1962, **62**, 145
22 Chaturvedi, P. N. *J. Mater. Sci. Lett.* 1987, **6**, 305
23 Kovacs, A. J. and Gonthier, A. *Kolloid Z. Z. Polym.* 1972, **250**, 530
24 Organ, S. J. and Keller, A. *J. Mater. Sci.* 1985, **20**, 1602
25 Organ, S. J. and Keller, A. *J. Polym. Sci.* (*B*) *Polym. Phys.* 1986, **24**, 2319
26 Hoffman, J. D. and Miller, R. L. *Macromolecules* 1989, **22**, 3502
27 Bassett, D. C. 'Principles of Polymer Morphology', Cambridge University Press, Cambridge, 1981, p. 55
28 Davis, G. T., Weeks, J. J., Martin, G. M. and Eby, R. K. *J. Appl. Phys.* 1974, **45**, 4175
29 Marand, H. *Macromolecules* 1989, **22**, 3980
30 Wittmann, J. C. and Lotz, B. *J. Polym. Sci., Polym. Phys. Edn.* 1985, **23**, 205
31 Mansfield, M. L. *Polymer* 1988, **29**, 1755
32 Mansfield, M. L. *Polym. Commun.* 1990, **31**, 283
33 Hoffman, J. D. and Miller, R. L. *Macromolecules* 1989, **22**, 3038
34 Davé, R. S. and Farmer, B. L. *Polymer* 1988, **29**, 1544
35 Miller, R. L. unpublished results
36 Alfonso, G. C., Falchetti, S. and Pedemonte, E. Europhys. Conf. Abstr.,1982, Vol. 6G, p. 49
37 Toda, A., Miyaji, H. and Kiho, H. *Polymer* 1986, **27**, 1505
38 Huseby, T. W. and Bair, H. E. *J. Appl. Phys.* 1968, **39**, 4969
39 Nakajima, A. and Hamada, F. *Pure Appl. Chem.* 1972, **31**, 1
40 Khoury, F., personal communication
41 Miller, R. L. *Kolloid Z. Z. Polym.* 1968, **225**, 62
42 Runt, J., Harrison, I. R., Varnell, W. D. and Wang, J.-I. *J. Macromol. Sci.* (*B*) 1983, **22**, 197
43 Bassett, D. C. and Hodge, A. M. *Proc. R. Soc. Lond.* (*A*) 1981, **377**, 25
44 Khoury, F. *Faraday Discuss. Chem. Soc.* 1979, **68**, 404
45 Bassett, D. C., Frank, F. C. and Keller, A. *Nature* 1959, **184**, 810
46 Bassett, D. C., Frank, F. C. and Keller, A. Proc. 2nd Eur. Reg. Conf. Electron Microscopy, 1960, Vol. 1, p. 244
47 Harrison, I. R. *J. Polym. Sci., Polym. Phys. Edn.* 1973, **11**, 991
48 Harrison, I. R. *J. Macromol. Sci., Chem.* (*A*) 1974, **8**, 43
49 Organ, S. J. and Keller, A. *J. Mater. Sci.* 1985, **20**, 1586
50 Organ, S. J., personal communication
51 Mansfield, M. L. *Macromolecules* 1983, **16**, 914
52 Kumar, S. K. and Yoon, D. Y. *Macromolecules* 1989, **22**, 3458
53 Patel, A. K. and Farmer, B. L. *Polymer* 1980, **21**, 153
54 Leung, W. M., Manley, R. S. J. and Panaras, A. R. *Macromolecules* 1985, **18**, 760
55 Organ, S. J. and Keller, A. *J. Polym. Sci.* (*C*) *Polym. Lett.* 1987, **25**, 67
56 DiCorleto, J. A. and Bassett, D. C. *Polymer* 1990, **31**, 1971
57 Hoffman, J. D. *Macromolecules* 1985, **18**, 772

Note added in proof

The solution of the Frank equations with moving boundary conditions given here is for the case $g > h$; Toda (*Polymer* in press) has obtained solutions for the case $g < h$ which lead to lenticular-like crystals where the subordinate growth front is curved but departs from being a section of an ellipse, especially near the apices.